JBC RESEARCH ARTICLE

Neurodevelopmental disorder mutations in the purine biosynthetic enzyme IMPDH2 disrupt its allosteric regulation

Received for publication, May 9, 2023, and in revised form, June 23, 2023 Published, Papers in Press, July 4, 2023,
https://doi.org/10.1016/j.jbc.2023.105012

Audrey G. O'Neill[1], Anika L. Burrell[1], Michael Zech[2,3], Orly Elpeleg[4,5], Tamar Harel[4,5], Simon Edvardson[6], Hagar Mor-Shaked[4,5], Alyssa L. Rippert[7], Tomoki Nomakuchi[7], Kosuke Izumi[7], and Justin M. Kollman[1,*]

From the [1]Department of Biochemistry, University of Washington, Seattle, Washington, USA; [2]Institute of Neurogenomics, Helmholtz Zentrum München, Munich, Germany; [3]Institute of Human Genetics, School of Medicine, Technical University of Munich, Munich, Germany; [4]Department of Genetics, Hadassah Medical Center, Jerusalem, Israel; [5]Faculty of Medicine, Hebrew University of Jerusalem, Jerusalem, Israel; [6]Alyn Hospital, Hebrew University School of Medicine, Jerusalem, Israel; [7]Division of Human Genetics, Children's Hospital of Philadelphia, Philadelphia, Pennsylvania, USA

Reviewed by members of the JBC Editorial Board. Edited by Enrique De La Cruz

Inosine 5′ monophosphate dehydrogenase (IMPDH) is a critical regulatory enzyme in purine nucleotide biosynthesis that is inhibited by the downstream product GTP. Multiple point mutations in the human isoform IMPDH2 have recently been associated with dystonia and other neurodevelopmental disorders, but the effect of the mutations on enzyme function has not been described. Here, we report the identification of two additional missense variants in *IMPDH2* from affected individuals and show that all of the disease-associated mutations disrupt GTP regulation. Cryo-EM structures of one IMPDH2 mutant suggest this regulatory defect arises from a shift in the conformational equilibrium toward a more active state. This structural and functional analysis provides insight into IMPDH2-associated disease mechanisms that point to potential therapeutic approaches and raises new questions about fundamental aspects of IMPDH regulation.

Dystonia is a neurological movement disorder associated with many different genetic variants. Recent studies have identified mutations in inosine 5′ monophosphate dehydrogenase (IMPDH) 2, a key regulatory enzyme in purine nucleotide biosynthesis, associated with dystonia and other neurodevelopmental disorders. Purine nucleotides are essential components of cells where they serve as signaling molecules, energy sources, and precursors of RNA and DNA. Purine salvage pathways function alongside *de novo* synthesis pathways to maintain purine pools during steady state, but *de novo* biosynthesis is upregulated during proliferation to meet increased purine demand (1, 2). IMPDH catalyzes the rate-limiting step of *de novo* guanine nucleotide biosynthesis—the conversion of inosine 5′-monophosphate (IMP) to xanthosine 5′-monophosphate (3, 4). Because IMP is also a precursor in the *de novo* synthesis of adenine nucleotides, IMPDH sits at a key metabolic branch point that controls flux between adenine and guanine nucleotide production (5–7).

To control this branch point, IMPDH is tightly regulated at multiple levels, including through allosteric regulation by purine nucleotide binding and reversible assembly into filaments (8–14) (Fig. 1). The IMPDH protomer consists of a catalytic domain and a regulatory Bateman domain, connected by a flexible hinge. IMPDH constitutively assembles tetramers through catalytic domain interactions, and tetramers reversibly dimerize into octamers through interactions of the Bateman domains in response to binding of ATP or GTP in three allosteric sites. Binding of ATP in sites one and two promotes Bateman domain interactions in an extended, active conformation. Binding of GTP in site two and site three, which is only formed in the compressed conformation, stabilizes a compressed, inactive conformation. Thus, GTP acts as an allosteric inhibitor by controlling the transition from extended to compressed conformations (9).

IMPDH2 is further regulated by assembly into filaments of stacked octamers, which reduces affinity for GTP by disfavoring the compressed conformation (12, 13). Filament formation is induced in cells under conditions with increased demand for guanine nucleotides, such as in response to IMPDH inhibition and starvation (15–22). In the presence of ATP, IMPDH filaments are conformationally heterogeneous, sampling a range of states between symmetrically extended and asymmetrically compressed. In the presence of GTP, the filaments more uniformly adopt a compressed conformation.

In humans, there are two IMPDH isozymes with 84% sequence identity (23). IMPDH1 is constitutively expressed in most cells as a housekeeping gene, while expression levels of IMPDH2 are higher in developing tissues (24, 25). IMPDH2 expression is also selectively enhanced in cancerous cells such as human brain tumors, sarcoma cells, and leukemic cells (24, 26–28). Both isoforms assemble filaments, but for IMPDH2 only, and incorporation into filaments reduces sensitivity of the enzyme to GTP inhibition by preventing complete compression of the octamer (13, 14).

Assembly of enzymes into filaments is a commonly observed mechanism that cells leverage to regulate metabolic processes (29–32). In general, filament assembly tunes

* For correspondence: Justin M. Kollman, jkoll@uw.edu.

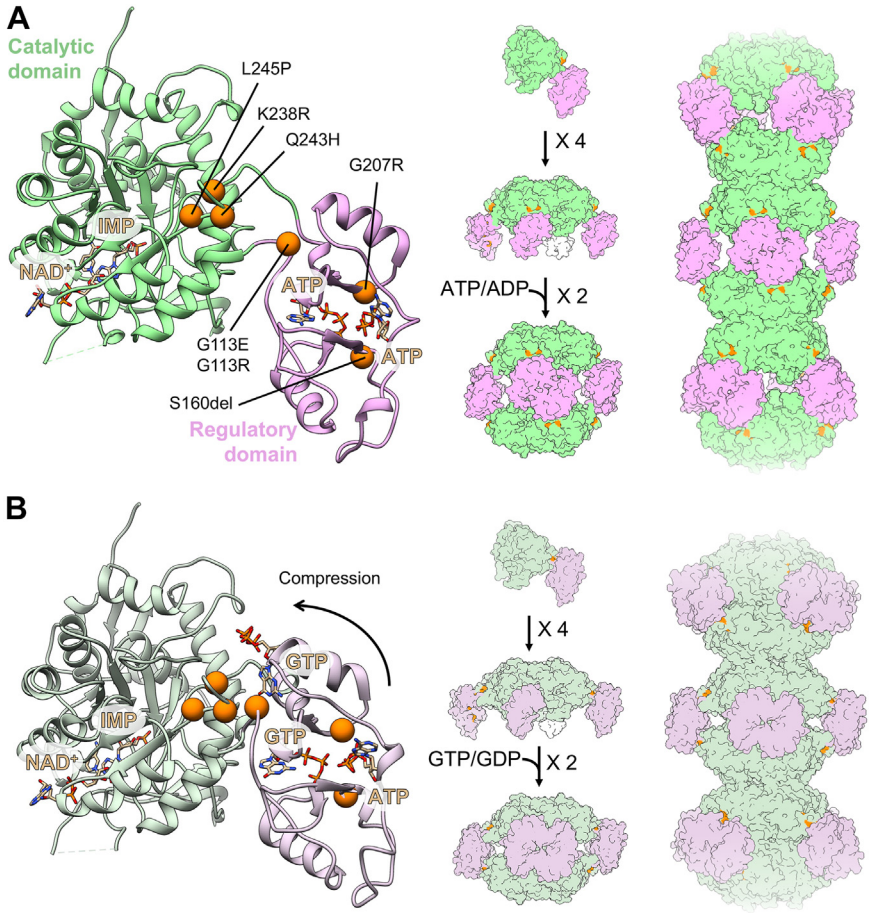

Figure 1. Locations of mutations in IMPDH2. Locations of all seven mutations (*orange*) are mapped to the IMPDH2 monomer in the extended, active state (*A*; PDB: 6U8N) and in the compressed, inhibited state (*B*; PDB: 6U9O). IMPDH2 monomers assemble into tetramers, octamers, and helical filamentous polymers with D4 symmetry. IMPDH, inosine 5′ monophosphate dehydrogenase; PDB, Protein Data Bank.

allosteric regulation and can serve to directly increase or decrease activity or alter sensitivity to allosteric regulators. Multiple homologs of the enzyme CTP synthase (CTPS) provide examples of the diversity of mechanisms by which polymerization can achieve different regulatory mechanisms—*Escherichia coli* CTPS filament assembly interactions directly stabilize an inhibited conformation (33), while human CTPS1 is maintained in a high activity conformation by assembly contacts (34). Human CTPS2 filaments function to dramatically increase the cooperativity of the transition between high and low activity conformations (35). Polymerization can also alter affinity for regulatory ligands, as in the case of human phosphoribosyl pyrophosphate synthetase 1, in which polymerization interactions stabilize an allosteric binding site, resulting in increased sensitivity to an allosteric activator (36). For IMPDH2, polymerization restricts compression of the octamers in the filament, affecting the equilibrium between extended and compressed states (12, 13). These reversible, assembly-based mechanisms of regulation allow the cell to rapidly and dynamically respond to changing metabolic needs.

Five mutations in *IMPDH2* were recently identified in patients with early onset neurodevelopmental diseases, including dystonia (37). All of the mutations are located in the regulatory domain or near the hinge that connects the regulatory and catalytic domains (Fig. 1). A series of similar mutations in *IMPDH1* have been associated with retinal degeneration (38–42), and a subset of these were recently shown to disrupt GTP feedback inhibition (14, 43). The role of IMPDH2 is believed to be essential for cell proliferation and growth, as KO of IMPDH2 in mice is embryonic lethal (44). Mice deficient in *IMPDH1* and also harboring a heterozygous deletion of *IMPDH2* had reduced IMPDH activity, but no developmental defects, supporting the hypothesis that IMPDH dysregulation, rather than a net decrease in its activity, is causative of disease (44, 45). However, more recently, a heterozygous early termination in exon 1 of *IMPDH2* was identified in a patient with dystonia (46), suggesting a decrease in IMPDH2 activity could also be causative of disease. Rare variants of IMPDH2 affecting the catalytic domain have also been identified in a cohort of dystonia patients of Chinese ancestry (47).

Here, we report two additional variants, L245P and K238R, of human *IMPDH2* associated with neurodevelopmental disease and show that neurodevelopmental disease-associated point mutations disrupt GTP feedback inhibition. Cryo-EM structures of the L245P mutant show that it can access both extended active and compressed inhibited conformations, but with the equilibrium between these conformational states disrupted relative to WT. We propose a mechanism of

dysregulation of the L245P variant in which the transition to the inhibited compressed state is disfavored. Other mutations result in a variety of structural phenotypes that suggest different mutations may have different molecular mechanisms of dysregulation.

Results

Identification of the L245P variant

The proband (Fig. 2), a three-year-old female, presented with global developmental delay, congenital anomalies (pulmonic stenosis and hip dysplasia), hypotonia, and dysmorphic features. The torticollis and abnormal posturing may be a form of dystonia in this patient. The clinical report of the patient is reported in Supporting Information.

Genetic evaluation in the proband included a chromosomal microarray, which did not identify any pathogenic or likely pathogenic genomic deletions or duplications, followed by trio exome sequencing. A *de novo* heterozygous variant was identified in *IMPDH2*: chr3:49064205[hg19]; NM_000884.3; c.734T > C; p.(Leu245Pro). This was confirmed by Sanger sequencing (Fig. 2). The variant is rare (not found in Genome Aggregation Database [gnomAD] or in the local database of ∼15,000 exomes), alters a conserved amino acid (Genomic Evolutionary Rate Profiling 5.97), has a high combined annotation-dependent depletion score of 29.7, and is predicted to be damaging by multiple bioinformatic algorithms (MutationTaster, Sorting Intolerant From Tolerant, Revel, and others). In addition, a *de novo* heterozygous variant was identified in low density lipoprotein receptor-related protein 1 (*LRP1*): chr12:57589465 [hg19]; c.8463dup; p.(Glu2822Ter). Pathogenic variants in *LRP1* have recently been associated with developmental dysplasia of the hip (48), and this variant therefore may have contributed to this phenotype in the proband.

Identification of the K238R variant

The proband is a now three-year-old male who presented to genetics evaluation at 9 months of age due to hypotonia and global developmental delays, including gross motor and speech delay. The clinical report of the patient is reported in the Supporting Information. Photos of the proband at different ages are shown in Fig. S1.

Chromosomal SNP microarray, Prader-Willi/Angelman syndrome methylation analysis, and metabolic screening labs were all performed and nondiagnostic. Exome sequencing was then recommended at 16 months of age and identified a *de novo*, likely pathogenic variant in *IMPDH2* (c.713A > G, p.Lys238Arg).

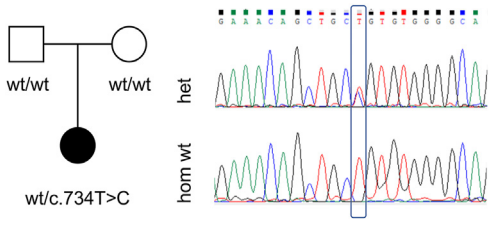

Figure 2. Genetic evaluation of the L245P variant. Pedigree of the proband with the *de novo* L245P variant of *IMPDH2* (*left*). Male individuals are represented by *squares*, and female individuals are represented by *circles*. Sanger sequencing confirmed the heterozygous c.734T > C mutation (*right*). IMPDH, inosine 5′ monophosphate dehydrogenase.

IMPDH2 variants are defective in GTP regulation

To determine whether disease-associated *IMPDH2* mutations have a direct effect on enzyme activity or regulation, we assayed purified recombinant enzymes *in vitro*. We observed modest variation in the apparent V_{max} of the enzymes and $K_{0.5}$ values for IMP and NAD+ among the IMPDH2 mutants relative to WT enzyme, suggesting that basal activity is not severely affected by the mutations (Table S1). We next tested whether the disease mutations affect GTP inhibition (Fig. 3). WT IMPDH2 filaments are inhibited by GTP with an IC_{50} of 577 μM under our assay conditions (Fig. 3); as previously reported, we find that IMPDH2 retains a basal level of activity even in the presence of saturating GTP (12, 13). Each mutant we tested retains significant activity up to 5 mM GTP (Fig. 3). While L245P, one of the mutations reported here, could be inhibited at much higher GTP concentrations, with an estimated IC_{50} of 7 mM, this value is far above the usual physiological concentration range of GTP (Fig. S2). Thus, each neurodevelopmental mutant dramatically compromises feedback inhibition by GTP, suggesting that disease phenotypes may be related to hyperactivity of IMPDH2 under conditions in which the WT enzyme would be inhibited.

Structural phenotypes of IMPDH2 mutants

The IMPDH2 neurodevelopmental mutations are in or near the regulatory domain, which controls the extended, compressed structural transition (Fig. 1). This led us to hypothesize that the loss of GTP regulation we observed arises from an inability to transition into the compressed, inhibited conformation. To assess changes to the structure and conformation in IMPDH2 mutants, we used negative stain EM. Under activating and inhibiting conditions for the WT enzyme, it is relatively straightforward to assess whether the enzyme is extended or compressed by directly observing the helical rise of filaments (12–14). Because the mutants have normal basal activity but are not inhibited by GTP, we anticipated that in the absence of GTP, the mutants should resemble the WT in the extended, active conformation. In the presence of GTP, which causes compression of WT filaments, we predicted we would not observe compression. However, negative stain analysis of IMPDH2 revealed surprising large-scale structural differences among the mutants (Fig. 4, Table S2).

First, we examined IMPDH2 mutant structures in the absence of GTP, where all mutants retain WT activity (Fig. 4*A*). Under this condition, G207R, Q243H, L245P, and K238R closely resemble WT in the canonical extended and active conformations. However, S160del did not assemble filaments at all, instead forming mostly tetramers in the presence of ATP. Surprisingly, both G113E and G113R are uniformly compressed, which has not previously been observed for IMPDH2 in the absence of GTP (9–13). More surprising still, in the presence of GTP, all of the disease mutants are able to

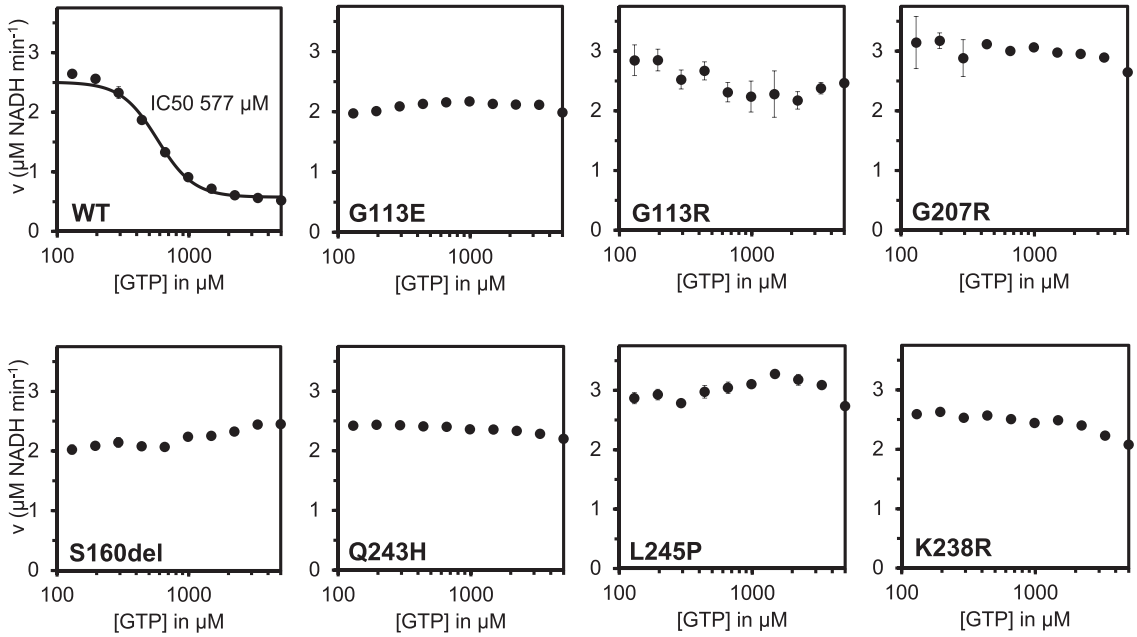

Figure 3. IMPDH2 neurodevelopmental variants disrupt GTP inhibition. GTP inhibition of WT IMPDH2 and IMPDH2 neurodevelopmental variants. Each data point represents the average initial rate of three reactions. Error bars represent standard deviation for n = 3 technical replicates. Velocities were calculated from the change in absorbance at 340 nm. Reactions were initiated with 300 μM NAD+ and contained 1 μM enzyme, 1 mM ATP, 1 mM IMP, 1 mM $MgCl_2$, and varying concentrations of GTP. IMP, inosine 5′ monophosphate; IMPDH, inosine 5′ monophosphate dehydrogenase.

assemble filaments in the compressed conformation, with the exception of S160del which forms only octamers, although it was not possible to directly measure whether GTP octamer are in the extended or compressed conformation (Fig. 4*B*). In all prior studies, a compressed conformation of IMPDH is associated with inhibition (9, 11–13), but the variants described here retain catalytic activity in the presence of GTP, suggesting that additional factors beyond compression must be required for IMPDH2 inhibition (Table S2).

Filament assembly reduces sensitivity of variants to GTP

We next investigated the effect of filament assembly on the variants' sensitivity to GTP. The engineered mutation Y12A at the filament assembly interface of IMPDH2 disrupts polymerization and increases sensitivity of IMPDH2 to GTP inhibition compared to the WT (12, 13). We introduced the Y12A mutation into each of the IMPDH2 mutants and confirmed with negative stain that the double mutants do not form filaments (Fig. S3). Next, we performed GTP inhibition assays on the double mutants. Because the S160del mutant does not form filaments at all, we anticipated that the Y12A mutation would not affect enzyme activity (Fig. 4). The S160del+Y12A mutant displayed no significant decrease in activity in the presence of GTP, as expected (Fig. 5). The other six double mutants display some inhibition at high GTP concentrations, with L245P + Y12A being the most sensitive (IC_{50} = 1.3 mM), followed by K238R + Y12A (IC_{50} = 1.9 mM). None of the double mutants were as sensitive to GTP inhibition as the nonassembly mutant alone (IC_{50} = 200 μM). This suggests that the mutations affect the octameric form of the enzyme as well, and assembly of the variants into filaments would further exacerbate downstream regulatory defects in the cell.

L245P filament structures reveal differences in flexibility

To investigate the structural basis for IMPDH2 dysregulation by neurodevelopmental mutations, we determined structures of L245P in the presence of ATP and GTP. We chose L245P as representative of the most common structural phenotype we observed with enzymes that undergo the extended to compressed transition in the presence of GTP despite retaining full activity (G207R, Q243H, L245P, and K238R).

First, we determined the structure of L245P in the catalytically active extended conformation in the absence of GTP. Flexibility in WT IMPDH2 filaments under these conditions arises from heterogeneity in the extended and compressed conformations of protomers within each octamer which can limit the resolution of cryo-EM structures. We previously developed an image processing strategy for the very flexible WT IMPDH2 filaments, which allows us to computationally separate uniformly extended filament segments from partially compressed (bent) filament segments (13). The approach also allows us to generate focused reconstructions of the repeating octameric subunit and the filament assembly interface. Following symmetry expansion and focused classification, we found that the majority of L245P segments were sorted into fully extended classes (73%) compared to only 17% fully extended WT IMPDH2 segments under these conditions (Fig. S4) (13). Thus, it appears that L245P reduces octamer flexibility in the active state, leading to a more uniformly extended structure than the very heterogeneous WT filaments.

The extended L245P structures refined to global resolutions that were significantly higher than our earlier WT structures—2.0 Å for the filament assembly interface and the catalytic core and 2.6 Å resolution for the octamer-centered reconstruction

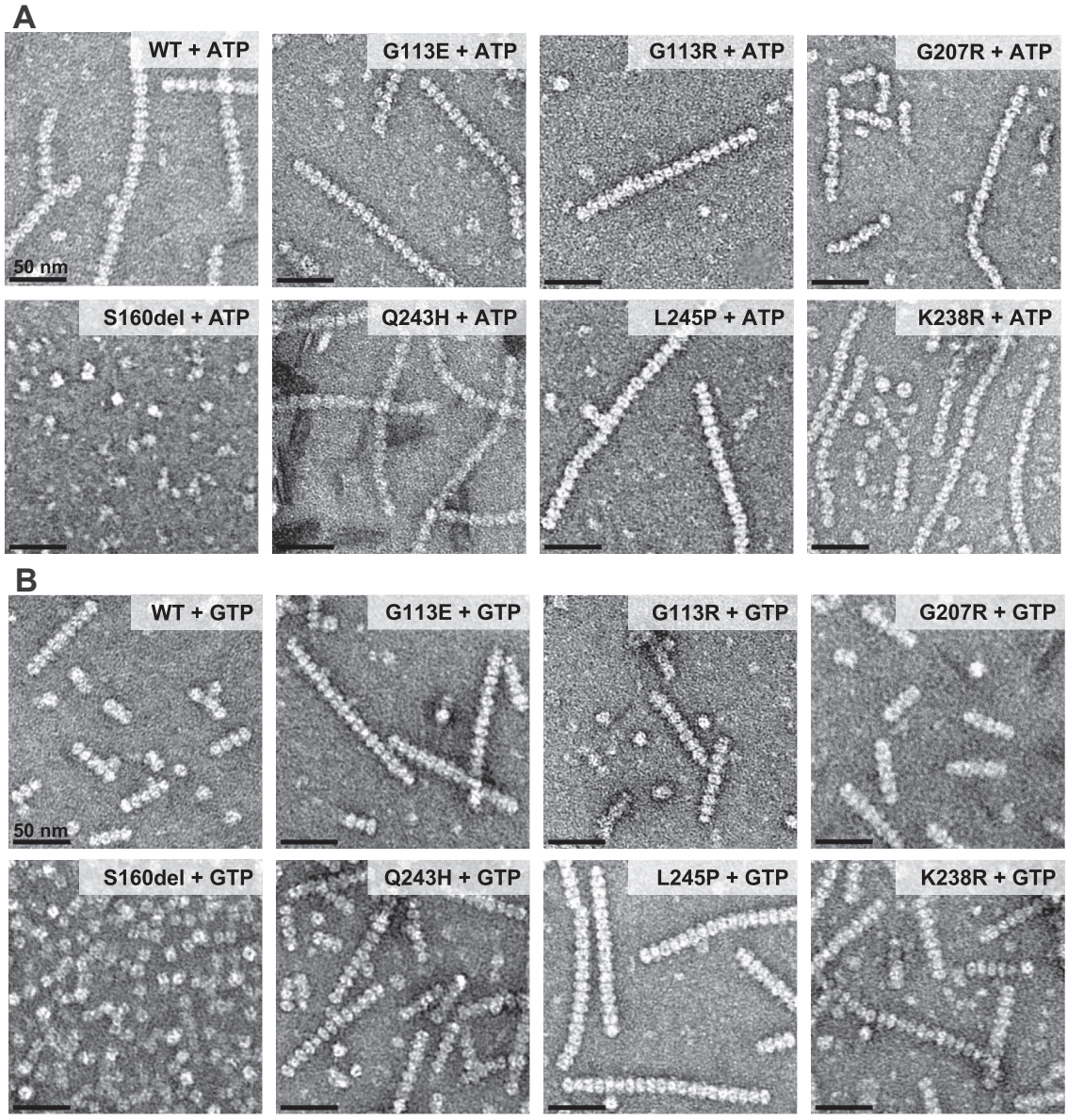

Figure 4. Negative stain EM reveals low-resolution differences between some mutants. Representative negative stain images of 2 μM enzyme with either 1 mM ATP and 1 mM $MgCl_2$ (*A*) or 5 mM GTP (*B*). The oligomeric and conformational states of some mutants vary from WT. S160del does not form filaments in either condition. G113E and G113R form compressed filaments in the absence of GTP.

(Figs. 6, *C* and *B* and S7). The mutation of L245 to proline is clear in the cryo-EM map and does not appear to perturb the conformation of the backbone around the mutation site relative to WT (Fig. 6*E*). IMP and NAD+ are clearly resolved in the active site, and ATP is well resolved in sites one and two in the regulatory domain (Fig. S5). Overall, the structures are nearly identical to the WT structure under this condition at the level of individual protomers, octamers, and the filament assembly interface (Fig. 6*D*). Some minor differences in loops of the regulatory domain likely reflect improved accuracy in model building at the improved resolution of the current reconstructions.

Next, we determined the structure of L245P in the presence of 20 mM GTP. At this high GTP concentration, we had previously observed that the WT IMPDH2 forms uniformly compressed filaments with no significant population of extended or bent octamers (13). However, from initial two-dimensional classification of L245P helical segments, it was clear that the mutant filaments were very heterogeneous (Fig. 7*A*). The data processing approach described above allowed us to separate out asymmetric bent segments, which closely resemble bent segments of WT IMPDH2 observed only in the absence of GTP (13). The remaining symmetrically compressed filament segments comprise only about 13% of the dataset (Fig. S6). Compared to the uniformly compressed WT, then, one consequence of the L245P mutation is to increase the heterogeneity of IMPDH2 filaments in the presence of GTP.

We used the symmetrically compressed filament segments to determine structures with global resolutions of 2.1 Å for the filament assembly interface and 3.0 Å for the octamer-centered reconstruction (Figs. S6–S8). We also determined a structure of the asymmetric, bent filament segment at a global resolution

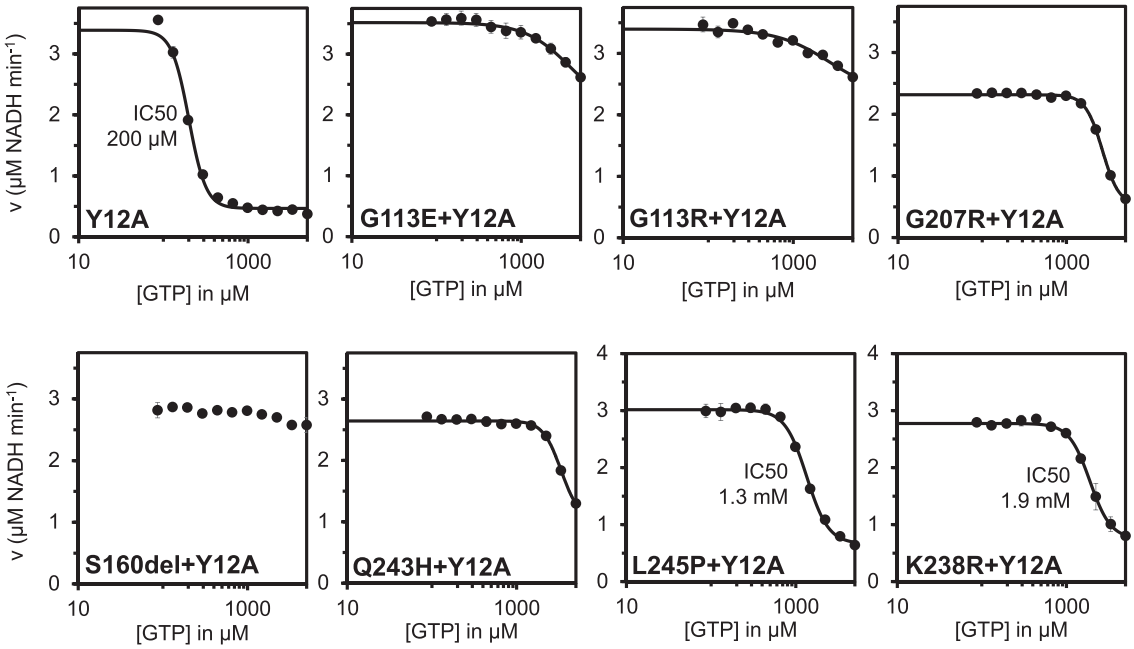

Figure 5. Mutations also disrupt GTP inhibition of free octamers. GTP inhibition curves of Y12A nonassembly mutant and Y12A/disease mutant double mutants of IMPDH2. Each data point represents the average initial rate of three reactions. Error bars represent standard deviation for n = 3 technical replicates. Velocities were calculated from the change in absorbance at 340 nm. Reactions were initiated with 300 μM NAD+ and contained 1 μM enzyme, 1 mM ATP, 1 mM IMP, 1 mM $MgCl_2$, and varying concentrations of GTP. IMP, inosine 5′ monophosphate; IMPDH, inosine 5′ monophosphate dehydrogenase.

of 2.7 Å (Figs. S6 and 7). Again, all ligands including GTP were well resolved (Fig. S5), and the filament interface was nearly identical to WT. The L245P protomer is also nearly identical to the WT protomer under this ligand condition (Fig. 7). Thus, IMPDH2-L245P can adopt a canonical compressed structure in the presence of GTP. However, under conditions that support uniform compression and inhibition of the WT enzyme, the mutant remains in an ensemble of partially compressed states.

Discussion

Maintenance of purine pools is critical in the central nervous system, where purine-based nucleotides and nucleosides have additional functions as second messengers, neurotransmitters, neuromodulators, and trophic agents (49–52). Purine nucleotide and nucleoside pools can be maintained by either salvage pathways or *de novo* pathways, but brain tissue relies primarily on salvage over *de novo* biosynthetic pathways (53). Genetic deficiencies in salvage pathway enzymes result in

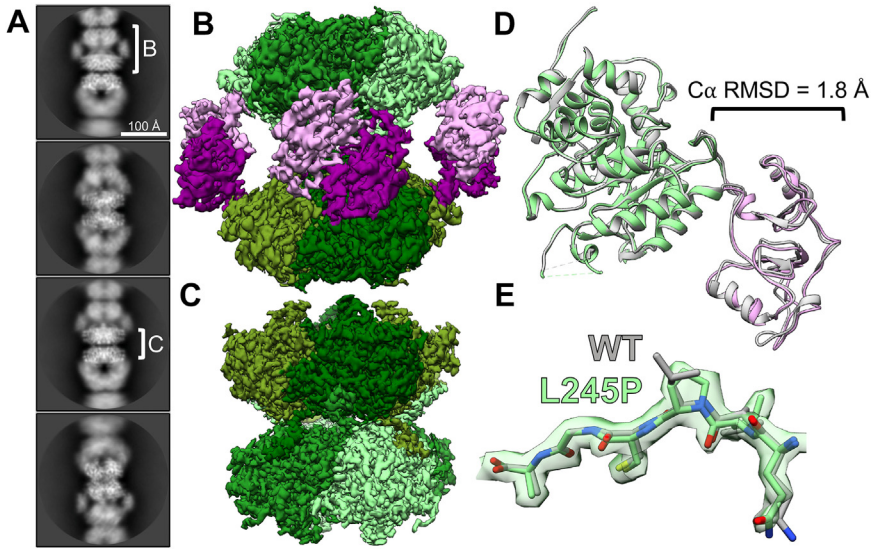

Figure 6. L245P mutant adopts similar extended conformation as the WT. Representative 2D class averages of L245P filaments in the presence of 1 mM ATP, 3 mM IMP, 5 mM NAD+, and 1 mM $MgCl_2$ (*A*). *White brackets* illustrate the regions on the filament where refinement was focused to produce reconstructions shown in *panels B* and *C*. Final cryo-EM reconstructions of octamer-centered (*B*) and interface-centered (*C*) filament segments. Regulatory domains are colored in shades of *pink*, and catalytic domains are *colored* in *shades* of *green*. Alignment of the L245P octamer-centered ribbon model (color; PDB 8G8F) to the WT ribbon model (*gray*; PDB 6U8N) at the catalytic domain (*green*). Calculation of C*α* RMSD at the regulatory domain (*pink*) shows minor differences in the structure of the monomer (*D*). The density around the mutation site shows that the backbone structure is not affected (*E*). IMP, inosine 5′ monophosphate; PDB, Protein Data Bank.

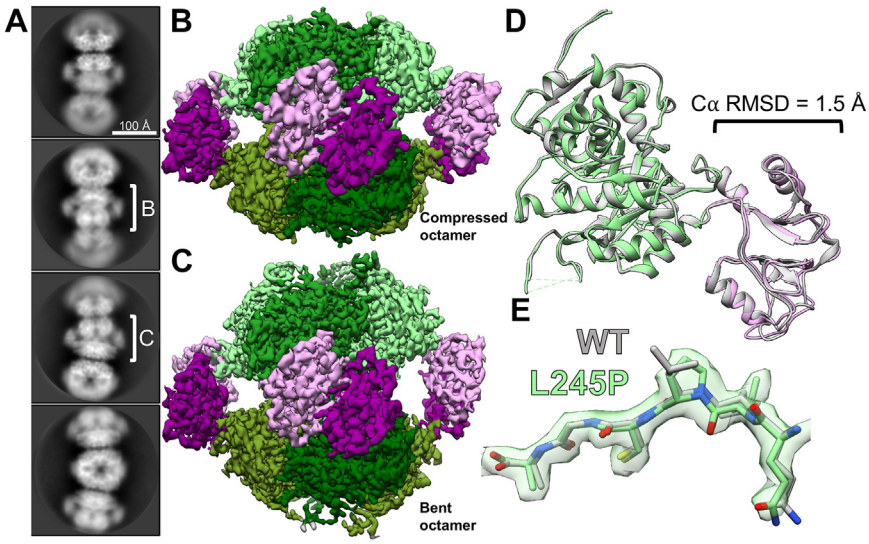

Figure 7. L245P filament is flexible in the presence of GTP. Representative 2D class averages of L245P filaments in the presence of 20 mM GTP, 1 mM ATP, 3 mM IMP, 5 mM NAD+, and 1 mM $MgCl_2$ (*A*). *White brackets* illustrate the regions on the filament where refinement was focused to produce reconstructions shown in *panels B* and *C*. Final cryo-EM reconstructions of straight octamer-centered (*B*) and bent octamer-centered (*C*) filament segments. Regulatory domains are colored in shades of *pink*, and catalytic domains are colored in shades of *green*. The filament assembly interface reconstruction is shown in Fig. S8. A model was built into the symmetrically compressed octamer reconstruction. Alignment of the L245P straight octamer-centered ribbon model (*color*; PDB 8G9B) to the WT ribbon model (*gray*; PDB 6U9O) at the catalytic domain (*green*). Calculation of C*α* RMSD at the regulatory domain (*pink*) again shows minor differences in the structure of the monomer (*D*). The density around the mutation site shows that the backbone structure is not affected (*E*). IMP, inosine 5′ monophosphate; PDB, Protein Data Bank.

increased flux through the *de novo* purine synthesis, leading to the neurodevelopmental disorder Lesch–Nyhan syndrome (54–57). The phenotype of this syndrome, including variably expressed generalized dystonia, motor disability, and cognitive disability, resembles phenotypes in cases of *IMPDH2* variants (37). In this study, we show that these IMPDH2 mutants all display insensitivity to allosteric inhibition by GTP, supporting the hypothesis that increased activity in the *de novo* purine biosynthetic pathway and subsequent perturbation of purine pools may lead to neurodevelopmental phenotypes.

Like *IMPDH2*, mutations in the gene for the other human isozyme, *IMPDH1*, also cause disease, in this case the retinal diseases Leber congenital amaurosis and retinitis pigmentosa (38–42). Like the *IMPDH2* mutations characterized here, a subset of *IMPDH1* mutations cluster near the allosteric domain or interdomain hinge and disrupt GTP inhibition (9, 14). Importantly, four of the five *IMPDH1* mutations that disrupt GTP regulation prevent IMPDH1 from adopting the compressed conformation, which we proposed as the mechanism of GTP dysregulation. We anticipated that the *IMPDH2* mutations studied here would have the same effect, but we were surprised to see that in each case we could measure, GTP appeared to cause compression of IMPDH2 in low-resolution negative stain micrographs (Fig. 4). Because these enzymes all retain high activity levels in the presence of GTP (Fig. 3), this result suggests that contrary to prior models, compression of IMPDH2 alone is not sufficient for allosteric inhibition.

IMPDH2-L245P structures provide insight into the seeming contradiction of the enzyme retaining WT activity in a compressed conformation. We found that the canonical extended and compressed states are virtually identical to the WT structures under the same conditions, including the binding of GTP to inhibitory allosteric sites. However, the conformational variability of filaments in different ligand states varies significantly. Active WT IMPDH2 is in an ensemble of structural states with different numbers of compressed and extended protomers within octamers giving rise to multiple bent conformations, and only a minority (17%) of octameric filament segments were classified as symmetrically extended (13). By comparison, the vast majority (73%) of L245P octamers are symmetrically extended, suggesting that one effect of the mutation is to rigidify the enzyme in the extended state. Conversely, under high concentrations of GTP, WT IMPDH2 octamers are uniformly compressed while only a minority of L245P octamers (13%) are fully compressed, the majority being in an ensemble of bent conformational states that resemble the active WT ensemble. That is, what appeared in low-resolution negative stain micrographs to be the compressed conformation was revealed to be an ensemble of partially compressed conformations using higher resolution cryo-EM approaches. Thus, L245P appears to disrupt GTP regulation by shifting the conformational equilibrium away from the inhibited, compressed conformation (Fig. 8).

Whether a disrupted conformational equilibrium underlies the GTP regulation defect for other IMPDH2 disease mutants remains to be determined, although our results suggest that some of the point mutations may work through different mechanisms. For example, S160del was the only mutation that disrupts filament assembly, which may play a role in its dysregulation. Because the seven mutations do not all lead to the same structural phenotypes at the level of polymerization or conformational state (Fig. 4), it will be important to characterize each one to elucidate mechanisms of disease for each. Understanding individual mechanisms of dysregulation may

also provide insight into variation in the onset and severity of disease phenotypes.

Additionally, two mutations at residue 113 appear to cause IMPDH2 to be constitutively in a compressed conformation in the absence of GTP. These mutations raise the question of how compressed IMPDH2 retains full WT levels of activity and suggests that compression alone is not sufficient to inactivate the enzyme. The G113E and G113R variants, therefore, may serve as a useful tool for dissecting previously unappreciated mechanisms of regulation of IMPDH2.

Assembly of IMPDH2 into filaments exacerbates the reduction in GTP sensitivity of the disease mutations. We have previously established the role for polymerization in reducing sensitivity to GTP inhibition, which increases the working range of the enzyme under conditions of elevated purine nucleotide demand (13, 14). When filament assembly was blocked, all of the point mutants partially restore sensitivity to GTP inhibition although not to WT levels (Fig. 5). The sensitivity to GTP inhibition of S160del, which itself prevents filament assembly, was not restored by introduction of our engineered nonassembly mutation Y12A.

Our results suggest potential therapeutic approaches that might be considered for treating patients with IMPDH2-associated developmental defects. The mutations are gain of function, allowing high levels of IMPDH activity at otherwise inhibitory concentrations of GTP. One approach might be the use of known IMPDH2 inhibitors to reduce the activity of the enzyme (58–60). Alternative approaches that target IMPDH2 assembly into filaments might also prove effective in some cases; for example, disrupting IMPDH2-L245P filament assembly reduces the IC_{50} for GTP into a more physiologically relevant range and might reduce activity sufficiently to be therapeutically useful. Future work investigating the treatment of IMPDH2 associated defects using inhibitors in cell-based systems and model organisms may prove fruitful.

In both *IMPDH1* and *IMPDH2*, disease-linked mutations in and around the Bateman domain result in the same type of biochemical defect affecting the nervous system. In the case of IMPDH1, this defect results in the degeneration of photoreceptors, possibly due to their unique dependence on IMPDH1 for ATP and cGMP (61–65). Imbalance of nucleotide pools in photoreceptors leads to photoreceptor death (66–68). In the case of IMPDH2, the defect results in neurodevelopmental disorders. In both cases, the dysregulation of IMPDH disrupts the delicate balance of purine pools in the nervous system.

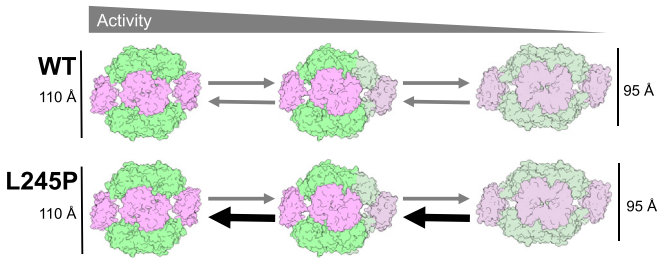

Figure 8. Model for the effect of L245P on IMPDH2 conformational equilibrium. WT IMPDH2 samples conformational space between fully extended and fully compressed octamers. L245P shifts that equilibrium to favor extended and bent conformations, resisting complete compression and maintaining activity. IMPDH, inosine 5′ monophosphate dehydrogenase.

Experimental procedures

Exome sequencing and Sanger validation of the IMPDH2 variants

Informed consent from the family of the individual with the L245P variant was obtained in accordance with Institutional Review Board-approved protocol 0306-10-HMO. After informed consent, genomic DNA was extracted from peripheral blood samples of the proband with the L245P variant and both parents. Exonic sequences were enriched in the DNA sample using the Integrated DNA Technologies xGen Exome Research Panel, V2.0 capture combined with xGen Human mitochondrial DNA Research Panel, v1.0 (Integrated DNA Technologies), and sequenced on a NovaSeq 6000 sequencing system (Illumina) as 100-bp paired-end runs. Data analysis including read alignment and variant calling was performed with DNAnexus software (Palo Alto) using default parameters, with the human genome assembly hg19/GRCh37 as reference. Variants were filtered out if they were off-target (intronic variants >8 bp from splice junction), synonymous (unless <4 bp from the splice site), or had minor allele frequency >0.01 in the Genome Aggregation Database or in our in-house exome database. The *IMPDH2* and *LRP1* variants were confirmed by Sanger sequencing in the affected individual and were not found in either parent. This work was done at Hadassah Medical Center, Jerusalem, Israel.

Genetic testing of the individual with the K238R variant was done as clinical trio exome sequencing through Invitae. Analysis of this data and evaluation of the patient were done at the Children's Hospital of Philadelphia. The patient was enrolled under Children's Hospital of Philadelphia Institutional Review Board approved protocol #16-013231. Written consent was obtained from parents for publication of photographs.

The studies in this work abide by the Declaration of Helsinki principles.

Recombinant IMPDH expression and purification

Purified IMPDH protein was prepared as described previously (12–14). Briefly, IMPDH2 variants were cloned into a pSMT3-Kan vector with an N-terminal 6xHis-SMT3/SUMO tag. Constructs were transformed into BL21 (DE3) *E. coli* and cultured in LB at 37 °C to an A_{600} of 0.9. Overexpression was induced with 1 mM IPTG for 4 h at 30 °C. Cells were collected by centrifugation. Cell pellets were resuspended at 4 °C in lysis buffer (50 mM KPO_4, 300 mM KCl, 10 mM imidazole, 800 mM urea, pH 8) with a dounce homogenizer, and the cells were lysed with an Emulsiflex-05 homogenizer. Lysate was cleared by centrifugation, and 6xHis-SMT3/SUMO tagged IMPDH2 was initially purified by Ni affinity chromatography using either a HisTrap FF column (GE HealthCare Life Sciences) on an Äkta Start chromatography system or a hand-packed HisPur Ni-NTA resin (Thermo Fisher Scientific),

eluting with 50 mM KPO_4, 300 mM KCl, 500 mM imidazole, pH 8. Fractions containing IMPDH2 were treated with 1 mg of purified ubiquitin-like specific protease 1 (ULP1) (69) per 100 mg IMPDH for 1 h at 4 °C to cleave the 6xHis-SMT3/SUMO tag. Following cleavage, 1 mM DTT and 800 mM urea were added to inhibit polymerization. Protein was concentrated using a 30,000 Dalton molecular weight cutoff Amicon filter and applied to a Superose 6 column pre-equilibrated in gel-filtration buffer (20 mM Hepes, 100 mM KCl, 800 mM urea, and 1 mM DTT, pH 8) using an Äkta Pure FPLC system. Peak fractions were concentrated using a 10,000 molecular weight cut-off Amicon filter, flash-frozen in liquid nitrogen, and stored in single use aliquots at −80 °C.

IMPDH activity assays

Protein aliquots were diluted in assay buffer (20 mM Hepes, 100 mM KCl, 1 mM DTT, pH 7.0) and pretreated with varying concentrations of ATP, GTP, and IMP for 15 min at 25 °C in a 96-well UV half-area transparent plates (Corning model 3679). Reactions (100 μl total) were initiated by addition of varying concentrations of NAD+. NADH production was measured over time in increments of 1 min for 15 min by absorbance at 340 nm using a Varioskan Lux microplate reader (Thermo Fisher Scientific) at 25 °C. Absorbance was correlated with NADH concentration using a standard curve. Specific activity was calculated by linear interpretation of the reaction slope for a 4 min window beginning 1 min after reaction initiation. All data points reported are an average of three measurements from the same protein preparation. Error bars are standard deviation. Fits for activity assays were calculated using the Hill–Langmuir equation $v = v_{max} * [S]^n / ((K0.5)^n + [S]^n)$ and IC_{50} was calculated using a modified Hill equation $V = V_{min} * (V_{max} - V_{min}) / (1 + (I/IC_{50})^{hill})$ (70).

Negatively stained electron microscopy

Samples were applied to glow-discharged continuous carbon EM grids and negatively stained with 2% uranyl formate. Grids were imaged by transmission electron microscopy using an FEI Morgagni at 100 kV acceleration voltage and a Gatan Orius charged-coupled device. Micrographs were collected at a nominal 22,000× magnification (pixel size 3.9 Å).

Electron cryo-microscopy sample preparation and data collection

Samples were applied to glow-discharged C-flat holey carbon EM grids (Protochips), blotted, and plunge-frozen in liquid ethane using a Vitrobot plunging apparatus (FEI) at 4 °C, 100% relative humidity. High-throughput data collection was performed using an FEI Titan Krios transmission electron microscope operating at 300 kV (equipped with a Gatan image filter and post-Gatan image filter Gatan K3 Summit direct electron detector) using the Leginon software package (71).

Electron cryo-microscopy image processing

Data collection parameters are summarized in Table S3. Movies were collected in super-resolution mode using Leginon, then aligned, and corrected for beam-induced motion using MotionCor2, with 2x Fourier binning and dose compensation applied during motion correction (71, 72). Contrast transfer function was estimated using CTFFIND4 (73). Relion 3.1 was used for all subsequent image processing (74, 75). Each dataset was individually processed using approximately the same previously published pipeline (13, 14).

Particles from a subset of 100 micrographs were manually picked from each dataset, extracted, and classified in 2D to generate templates for autopicking. Particles were autopicked using these templates, extracted with a box size of 400 Å, with 4x binning, and classified in 2D to remove junk. For initial 3D refinement, a previous IMPDH filament reconstruction was accessed from the Electron Microscopy Data Bank (EMDB) (EMD-20742 for the dataset with GTP, or EMD-20687 for the dataset without GTP) was low-pass filtered to 40 Å and used as an initial reference to align the particles at the filament assembly interface.

As described previously, two different locations along the D4-symmetric IMPDH filament may be used as symmetry origins—the center of the octameric filament segment or the center of the filament assembly interface (13, 14). Briefly, binned particles were initially aligned to a low-pass filtered IMPDH filament volume centered on the desired symmetry origin as a reference in an initial round of 3D autorefinement, given a large offset range of 25. Helical segments were processed as single particles. Helical symmetry was not applied. After initial binned refinement, particles were unbinned and re-extracted with a pixel size of 0.843 Å, followed by 2D classification. Selected particles were submitted to 3D autorefinement with D4 symmetry imposed. Remaining heterogeneity was removed with subsequent rounds of 3D classification.

Contrast transfer function refinement and particle polishing were performed to refine per-particle defocus and per-micrograph astigmatism. Partial signal subtraction of the poorly resolved particle ends was performed on either the filament assembly interface or the octameric filament segment to boost resolution of the centered region. To this end, a mask was applied over either the central eight catalytic domains of the filament assembly interface or over the eight monomers of the octameric filament segment, and signal outside of the masks was subtracted. The resulting map was autorefined in 3D. 2D and 3D classification while skip_align was performed to remove residual heterogeneity.

Model building and refinement

Structures of human IMPDH2 filaments in the extended conformation (Protein Data Bank [PDB] 6U8N for the octamer-centered reconstruction and PDB 6U8E for the interface-centered reconstruction) and the compressed conformation (PDB 6U9O for the octamer-centered reconstruction and PDB 6U8S for the interface-centered reconstruction) were used as templates for model building. Templates were rigid-body fit into the cryo-EM maps using UCSF Chimera, and phenix.real_space_refine was used for automated fitting employing rigid-body refinement, noncrystallographic symmetry constraints,

gradient-driven minimization and simulated annealing (76). Outputs from real-space refinement in PHENIX were inspected and manually adjusted with semiautomated fitting in ISOLDE and manual fitting in Coot (77, 78). This process was repeated iteratively, improving Molprobity statistics and fit to density. Refinement statistics are summarized in Table S3. Structure figures were prepared using UCSF Chimera (79).

Data availability

The coordinates are deposited in the Protein Data Bank with PDB IDs 8FOZ (interface-centered extended hIMPDH2-L245P), 8G8F (octamer-centered extended hIMPDH2-L245P), 8FUZ (interface-centered compressed hIMPDH2-L245P), and 8G9B (octamer-centered compressed hIMPDH2-L245P). The cryo-EM maps are deposited in the Electron Microscopy Data Bank with IDs EMD-29357 (interface-centered extended hIMPDH2-L245P), EMD-29848 (octamer-centered extended hIMPDH2-L245P), EMD-29482 (interface-centered compressed hIMPDH2-L245P), EMD-29863 (octamer-centered compressed hIMPDH2-L245P), and EMD-29870 (octamer-centered bent hIMPDH2-L245P). All other data are available in the main text or the supporting information.

Supporting information—This article contains supporting information.

Acknowledgments—We thank the patients and the family of the patients for participating in the study. We thank the Arnold and Mabel Beckman Cryo-EM Center at the University of Washington for electron microscope use.

Author contributions—A. G. O. N., A. L. B., M. Z., and J. M. K. conceptualization; A. G. O. N. and A. L. B. validation; A. G. O. N. and A. L. B. formal analysis; A. G. O. N., A. L. B., O. E., T. H., S. E., H. M. S., A. L. R., T. N., and K. I., investigation; A. G. O. N. and J. M. K. writing–original draft; A. G. O. N., A. L. B., M. Z., O. E., T. H., S. E., H. M. S., A. L. R., and J. M. K. writing–review and editing; A. G. O. N., T. H., and A. L. R., visualization; A. G. O. N., A. L. B., M. Z., and J. M. K. funding acquisition; O. E., S. E., H. M. S., A. L. R., T. N., K. I. and J. M. K. resources; J. M. K. supervision; J. M. K. project administration.

Funding and additional information—This work was supported by the US National Institutes of Health (R01GM118396 and S10OD023476 to J. M. K., T32GM008268 to A. G. O., and F31EY030732 to A. L. B.), and the German Research Foundation (DFG 458949627; ZE 1213/2-1 to M. Z.). The content is solely the responsibility of the authors and does not necessarily represent the official views of the National Institutes of Health.

Conflict of interest—The authors declare that they have no conflicts of interest with the contents of this article.

Abbreviations—The abbreviations used are: CTPS, CTP synthase; IMP, inosine 5′ monophosphate; IMPDH, inosine 5′ monophosphate dehydrogenase; LRP1, low density lipoprotein receptor-related protein 1; PDB, Protein Data Bank.

References

1. Jackson, R. C., Morris, H. P., and Weber, G. (1977) Enzymes of the purine ribonucleotide cycle in rat hepatomas and kidney tumors. *Cancer Res.* **37**, 3057–3065
2. Mayer, D., Natsumeda, Y., Ikegami, T., Faderan, M., Lui, M., Emrani, J., *et al.* (1990) Expression of key enzymes of purine and pyrimidine metabolism in a hepatocyte-derived cell line at different phases of the growth cycle. *J. Cancer Res. Clin. Oncol.* **116**, 251–258
3. Jackson, R. C., Weber, G., and Morris, H. P. (1975) IMP dehydrogenase, an enzyme linked with proliferation and malignancy. *Nature* **256**, 331–333
4. Natsumeda, Y., Ikegami, T., Murayama, K., and Weber, G. (1988) De novo Guanylate synthesis in the commitment to replication in Hepatoma 3924A cells1. *Cancer Res.* **48**, 507–511
5. Glesne, D. A., Collart, F. R., and Huberman, E. (1991) Regulation of IMP dehydrogenase gene expression by its end products, guanine nucleotides. *Mol. Cell. Biol.* **11**, 5417–5425
6. Jain, J., Almquist, S. J., Ford, P. J., Shlyakhter, D., Wang, Y., Nimmesgern, E., *et al.* (2004) Regulation of inosine monophosphate dehydrogenase type I and type II isoforms in human lymphocytes. *Biochem. Pharmacol.* **67**, 767–776
7. Dayton, J. S., Lindsten, T., Thompson, C. B., and Mitchell, B. S. (1994) Effects of human T lymphocyte activation on inosine monophosphate dehydrogenase expression. *J. Immunol.* **152**, 984–991
8. Scott, J. W., Hawley, S. A., Green, K. A., Anis, M., Stewart, G., Scullion, G. A., *et al.* (2004) CBS domains form energy-sensing modules whose binding of adenosine ligands is disrupted by disease mutations. *J. Clin. Invest.* **113**, 274–284
9. Buey, R. M., Ledesma-Amaro, R., Velázquez-Campoy, A., Balsera, M., Chagoyen, M., de Pereda, J. M., *et al.* (2015) Guanine nucleotide binding to the bateman domain mediates the allosteric inhibition of eukaryotic IMP dehydrogenases. *Nat. Commun.* **6**, 8923
10. Labesse, G., Alexandre, T., Vaupré, L., Salard-Arnaud, I., Him, J. L. K., Raynal, B., *et al.* (2013) MgATP regulates allostery and fiber formation in IMPDHs. *Structure* **21**, 975–985
11. Buey, R. M., Fernández-Justel, D., Marcos-Alcalde, Í., Winter, G., Gómez-Puertas, P., de Pereda, J. M., *et al.* (2017) A nucleotide-controlled conformational switch modulates the activity of eukaryotic IMP dehydrogenases. *Sci. Rep.* **7**, 2648
12. Anthony, S. A., Burrell, A. L., Johnson, M. C., Duong-Ly, K. C., Kuo, Y.-M., Simonet, J. C., *et al.* (2017) Reconstituted IMPDH polymers accommodate both catalytically active and inactive conformations. *Mol. Biol. Cell* **28**, 2600–2608
13. Johnson, M. C., and Kollman, J. M. (2020) Cryo-EM structures demonstrate human IMPDH2 filament assembly tunes allosteric regulation. *Elife* **9**, e53243
14. Burrell, A. L., Nie, C., Said, M., Simonet, J. C., Fernández-Justel, D., Johnson, M. C., *et al.* (2022) IMPDH1 retinal variants control filament architecture to tune allosteric regulation. *Nat. Struct. Mol. Biol.* **29**, 47–58
15. Ji, Y., Gu, J., Makhov, A. M., Griffith, J. D., and Mitchell, B. S. (2006) Regulation of the interaction of inosine monophosphate dehydrogenase with mycophenolic acid by GTP. *J. Biol. Chem.* **281**, 206–212
16. Gunter, J. H., Thomas, E. C., Lengefeld, N., Kruger, S. J., Worton, L., Gardiner, E. M., *et al.* (2008) Characterisation of inosine monophosphate dehydrogenase expression during retinal development: differences between variants and isoforms. *Int. J. Biochem. Cell Biol.* **40**, 1716–1728
17. Thomas, E. C., Gunter, J. H., Webster, J. A., Schieber, N. L., Oorschot, V., Parton, R. G., *et al.* (2012) Different characteristics and nucleotide binding properties of inosine monophosphate dehydrogenase (IMPDH) isoforms. *PLoS One* **7**, e51096
18. Carcamo, W. C., Calise, S. J., von Mühlen, C. A., Satoh, M., and Chan, E. K. L. (2014) Molecular cell biology and immunobiology of mammalian rod/ring structures. *Int. Rev. Cell Mol. Biol.* **308**, 35–74
19. Calise, S. J., Carcamo, W. C., Krueger, C., Yin, J. D., Purich, D. L., and Chan, E. K. L. (2014) Glutamine deprivation initiates reversible assembly of mammalian rods and rings. *Cell. Mol. Life Sci.* **71**, 2963–2973
20. Duong-Ly, K. C., Kuo, Y.-M., Johnson, M. C., Cote, J. M., Kollman, J. M., Soboloff, J., *et al.* (2018) T cell activation triggers reversible inosine-5′-monophosphate dehydrogenase assembly. *J. Cell Sci.* **131**, jcs223289

21. Juda, P., Šmigová, J., Kováčik, L., Bártová, E., and Raška, I. (2014) Ultrastructure of Cytoplasmic and nuclear inosine-5′-monophosphate dehydrogenase 2 "rods and rings" Inclusions. *J. Histochem. Cytochem.* **62**, 739–750
22. Ahangari, N., Munoz, D. G., Coulombe, J., Gray, D. A., Engle, E. C., Cheng, L., *et al.* (2021) Nuclear IMPDH filaments in human Gliomas. *J. Neuropathol. Exp. Neurol.* **80**, 944–954
23. Natsumeda, Y., Ohno, S., Kawasaki, H., Konno, Y., Weber, G., and Suzuki, K. (1990) Two distinct cDNAs for human IMP dehydrogenase. *J. Biol. Chem.* **265**, 5292–5295
24. Senda, M., and Natsumeda, Y. (1994) Tissue-differential expression of two distinct genes for human IMP dehydrogenase (E.C.1.1.1.205). *Life Sci.* **54**, 1917–1926
25. Peng, M., Li, S., He, Q., Zhao, J., Li, L., and Ma, H. (2018) Proteomics reveals changes in hepatic proteins during chicken embryonic development: an alternative model to study human obesity. *BMC Genomics* **19**, 29
26. Konno, Y., Natsumeda, Y., Nagai, M., Yamaji, Y., Ohno, S., Suzuki, K., *et al.* (1991) Expression of human IMP dehydrogenase types I and II in Escherichia coli and distribution in human normal lymphocytes and leukemic cell lines. *J. Biol. Chem.* **266**, 506–509
27. Nagai, M., Natsumeda, Y., Konno, Y., Hoffman, R., Irino, S., and Weber, G. (1991) Selective up-regulation of type II inosine 5′-monophosphate dehydrogenase messenger RNA expression in human Leukemias1. *Cancer Res.* **51**, 3886–3890
28. Collart, F. R., Chubb, C. B., Mirkin, B. L., and Huberman, E. (1992) Increased inosine-5′-phosphate dehydrogenase gene expression in solid tumor tissues and tumor cell lines. *Cancer Res.* **52**, 5826–5828
29. Peterson, J., Akizu, N., Simonet, J., Foster, M., and O'Reilly, A. (2020) Enzyme polymerization in nucleotide biosynthesis. *FASEB J.* **34**, 1
30. Simonet, J. C., Burrell, A. L., Kollman, J. M., and Peterson, J. R. (2020) Freedom of assembly: metabolic enzymes come together. *Mol. Biol. Cell* **31**, 1201–1205
31. Lynch, E. M., Kollman, J. M., and Webb, B. A. (2020) Filament formation by metabolic enzymes—a new twist on regulation. *Curr. Opin. Cell Biol.* **66**, 28–33
32. Hvorecny, K. L., and Kollman, J. M. (2023) Greater than the sum of parts: mechanisms of metabolic regulation by enzyme filaments. *Curr. Opin. Struct. Biol.* **79**, 102530
33. Barry, R. M., Bitbol, A.-F., Lorestani, A., Charles, E. J., Habrian, C. H., Hansen, J. M., *et al.* (2014) Large-scale filament formation inhibits the activity of CTP synthetase. *Elife* **3**, e03638
34. Lynch, E. M., Hicks, D. R., Shepherd, M., Endrizzi, J. A., Maker, A., Hansen, J. M., *et al.* (2017) Human CTP synthase filament structure reveals the active enzyme conformation. *Nat. Struct. Mol. Biol.* **24**, 507–514
35. Lynch, E. M., and Kollman, J. M. (2020) Coupled structural transitions enable highly cooperative regulation of human CTPS2 filaments. *Nat. Struct. Mol. Biol.* **27**, 42–48
36. Hvorecny, K. L., Hargett, K., Quispe, J. D., and Kollman, J. M. (2023) Human PRPS1 filaments stabilize allosteric sites to regulate activity. *Nat. Struct. Mol. Biol.* **30**, 391–402
37. Zech, M., Jech, R., Boesch, S., Škorvánek, M., Weber, S., Wagner, M., *et al.* (2020) Monogenic variants in dystonia: an exome-wide sequencing study. *Lancet Neurol.* **19**, 908–918
38. Bowne, S. J. (2002) Mutations in the inosine monophosphate dehydrogenase 1 gene (IMPDH1) cause the RP10 form of autosomal dominant retinitis pigmentosa. *Hum. Mol. Genet.* **11**, 559–568
39. Kennan, A. (2002) Identification of an IMPDH1 mutation in autosomal dominant retinitis pigmentosa (RP10) revealed following comparative microarray analysis of transcripts derived from retinas of wild-type and Rho-/- mice. *Hum. Mol. Genet.* **11**, 547–558
40. Wada, Y., Sandberg, M. A., McGee, T. L., Stillberger, M. A., Berson, E. L., and Dryja, T. P. (2005) Screen of the *IMPDH1* gene among patients with dominant retinitis pigmentosa and clinical Features associated with the most common mutation, Asp226Asn. *Invest. Ophthalmol. Vis. Sci.* **46**, 1735
41. Grover, S., Fishman, G. A., and Stone, E. M. (2004) A novel IMPDH1 mutation (Arg231Pro) in a family with a severe form of autosomal dominant retinitis pigmentosa. *Ophthalmology* **111**, 1910–1916
42. Bowne, S. J., Sullivan, L. S., Mortimer, S. E., Hedstrom, L., Zhu, J., Spellicy, C. J., *et al.* (2006) Spectrum and frequency of mutations in IMPDH1 associated with autosomal dominant retinitis pigmentosa and Leber congenital amaurosis. *Invest. Ophthalmol. Vis. Sci.* **47**, 34
43. Fernández-Justel, D., Núñez, R., Martín-Benito, J., Jimeno, D., González-López, A., Soriano, E. M., *et al.* (2019) A nucleotide-dependent conformational switch controls the polymerization of human IMP dehydrogenases to modulate their catalytic activity. *J. Mol. Biol.* **431**, 956–969
44. Gu, J. J., Stegmann, S., Gathy, K., Murray, R., Laliberte, J., Ayscue, L., *et al.* (2000) Inhibition of T lymphocyte activation in mice heterozygous for loss of the IMPDH II gene. *J. Clin. Invest.* **106**, 599–606
45. Gu, J. J., Tolin, A. K., Jain, J., Huang, H., Santiago, L., and Mitchell, B. S. (2003) Targeted disruption of the inosine 5′-monophosphate dehydrogenase type I gene in mice. *Mol. Cell. Biol.* **23**, 6702–6712
46. Kuukasjärvi, A., Landoni, J. C., Kaukonen, J., Juhakoski, M., Auranen, M., Torkkeli, T., *et al.* (2021) IMPDH2: a new gene associated with dominant juvenile-onset dystonia-tremor disorder. *Eur. J. Hum. Genet.* **29**, 1833–1837
47. Lin, J., Li, C., Cui, Y., Hou, Y., Zhang, L., Ou, R., *et al.* (2023) Rare variants in IMPDH2 cause autosomal dominant dystonia in Chinese population. *J. Neurol.* **270**, 2197–2203
48. Yan, W., Zheng, L., Xu, X., Hao, Z., Zhang, Y., Lu, J., *et al.* (2022) Heterozygous LRP1 deficiency causes developmental dysplasia of the hip by impairing triradiate chondrocytes differentiation due to inhibition of autophagy. *Proc. Natl. Acad. Sci. U. S. A.* **119**, e2203557119
49. Deutsch, S. I., Long, K. D., Rosse, R. B., Mastropaolo, J., and Eller, J. (2005) Hypothesized deficiency of guanine-based purines may contribute to abnormalities of neurodevelopment, neuromodulation, and neurotransmission in lesch-nyhan syndrome. *Clin. Neuropharmacol.* **28**, 28–37
50. Frizzo, M. E., Lara, D. R., Dahm, K. C., Prokopiuk, A. S., Swanson, R. A., and Souza, D. O. (2001) Activation of glutamate uptake by guanosine in primary astrocyte cultures. *Neuroreport* **12**, 879–881
51. Rathbone, M. P., Middlemiss, P. J., Gysbers, J. W., Andrew, C., Herman, M. A. R., Reed, J. K., *et al.* (1999) Trophic effects of purines in neurons and glial cells. *Prog. Neurobiol.* **59**, 663–690
52. Long, H., Cameron, S., Yu, L., and Rao, Y. (2006) *De novo* GMP synthesis is required for Axon guidance in drosophila. *Genetics* **172**, 1633–1642
53. Rosenbloom, F. M. (1967) Inherited disorder of purine metabolism: correlation between central nervous system Dysfunction and biochemical defects. *JAMA* **202**, 175
54. Seegmiller, J. E., Rosenbloom, F. M., and Kelley, W. N. (1967) Enzyme defect associated with a Sex-linked human neurological disorder and excessive purine synthesis. *Science* **155**, 1682–1684
55. Lesch, M., and Nyhan, W. L. (1964) A familial disorder of uric acid metabolism and central nervous system function. *Am. J. Med.* **36**, 561–570
56. Rosenbloom, F. M., Henderson, J. F., Caldwell, I. C., Kelley, W. N., and Seegmiller, J. E. (1968) Biochemical bases of accelerated purine biosynthesis de novo in human fibroblasts lacking hypoxanthine-guanine phosphoribosyltransferase. *J. Biol. Chem.* **243**, 1166–1173
57. Wood, A. W., Becker, M. A., Minna, J. D., and Seegmiller, J. E. (1973) Purine metabolism in normal and Thioguanine-Resistant Neuroblastoma. *Proc. Natl. Acad. Sci. U. S. A.* **70**, 3880–3883
58. Franklin, T. J., and Cook, J. M. (1969) The inhibition of nucleic acid synthesis by mycophenolic acid. *Biochem. J.* **113**, 515–524
59. Sintchak, M. D., Fleming, M. A., Futer, O., Raybuck, S. A., Chambers, S. P., Caron, P. R., *et al.* (1996) Structure and mechanism of inosine monophosphate dehydrogenase in complex with the Immunosuppressant mycophenolic acid. *Cell* **85**, 921–930
60. Liao, L.-X., Song, X.-M., Wang, L.-C., Lv, H.-N., Chen, J.-F., Liu, D., *et al.* (2017) Highly selective inhibition of IMPDH2 provides the basis of antineuroinflammation therapy. *Proc. Natl. Acad. Sci. U. S. A.* **114**, E5986–E5994
61. Wong-Riley, M. (2010) Energy metabolism of the visual system. *Eye Brain* **2**, 99–116
62. Country, M. W. (2017) Retinal metabolism: a comparative look at energetics in the retina. *Brain Res.* **1672**, 50–57

63. Arshavsky, V. Y., and Burns, M. E. (2012) Photoreceptor signaling: supporting vision across a wide range of Light Intensities. *J. Biol. Chem.* **287**, 1620–1626
64. Luo, D.-G., Xue, T., and Yau, K.-W. (2008) How vision begins: an odyssey. *Proc. Natl. Acad. Sci. U. S. A.* **105**, 9855–9862
65. Palczewski, K. (2014) Chemistry and biology of the initial steps in vision: the friedenwald lecture. *Invest. Ophthalmol. Vis. Sci.* **55**, 6651
66. Sharma, A. K., and Rohrer, B. (2007) Sustained elevation of Intracellular cGMP causes oxidative stress triggering calpain-mediated apoptosis in photoreceptor degeneration. *Curr. Eye Res.* **32**, 259–269
67. Du, J., An, J., Linton, J. D., Wang, Y., and Hurley, J. B. (2018) How Excessive cGMP Impacts metabolic proteins in retinas at the onset of degeneration. In: Ash, J. D., Anderson, R. E., LaVail, M. M., Bowes Rickman, C., Hollyfield, J. G., Grimm, C., eds.**, 1074**. *Retinal Degenerative Diseases*, Springer International Publishing, Cham: 289–295. Advances in Experimental Medicine and Biology
68. Charish, J. (2019) cAMP and photoreceptor cell death in retinal degeneration. In: Bowes Rickman, C., Grimm, C., Anderson, R. E., Ash, J. D., LaVail, M. M., Hollyfield, J. G., eds.**, 1185**. *Retinal Degenerative Diseases*, Springer International Publishing, Cham: 301–304. Advances in Experimental Medicine and Biology
69. Mossessova, E., and Lima, C. D. (2000) Ulp1-SUMO Crystal structure and genetic analysis reveal conserved interactions and a regulatory element essential for cell growth in yeast. *Mol. Cell* **5**, 865–876
70. Volpe, D. A., Hamed, S. S., and Zhang, L. K. (2014) Use of different parameters and equations for calculation of IC50 values in Efflux assays: potential sources of variability in IC50 determination. *AAPS J.* **16**, 172–180
71. Carragher, B., Kisseberth, N., Kriegman, D., Milligan, R. A., Potter, C. S., Pulokas, J., *et al.* (2000) Leginon: an automated system for acquisition of images from vitreous ice specimens. *J. Struct. Biol.* **132**, 33–45
72. Zheng, S. Q., Palovcak, E., Armache, J.-P., Verba, K. A., Cheng, Y., and Agard, D. A. (2017) MotionCor2: anisotropic correction of beam-induced motion for improved cryo-electron microscopy. *Nat. Methods* **14**, 331–332
73. Rohou, A., and Grigorieff, N. (2015) CTFFIND4: fast and accurate defocus estimation from electron micrographs. *J. Struct. Biol.* **192**, 216–221
74. Scheres, S. H. W. (2012) RELION: implementation of a bayesian approach to cryo-EM structure determination. *J. Struct. Biol.* **180**, 519–530
75. Zivanov, J., Nakane, T., Forsberg, B. O., Kimanius, D., Hagen, W. J., Lindahl, E., *et al.* (2018) New tools for automated high-resolution cryo-EM structure determination in RELION-3. *Elife* **7**, e42166
76. Afonine, P. V., Poon, B. K., Read, R. J., Sobolev, O. V., Terwilliger, T. C., Urzhumtsev, A., *et al.* (2018) Real-space refinement in *PHENIX* for cryo-EM and crystallography. *Acta Crystallogr. D Struct. Biol.* **74**, 531–544
77. Croll, T. I. (2018) *Isolde* : a physically realistic environment for model building into low-resolution electron-density maps. *Acta Crystallogr. D Struct. Biol.* **74**, 519–530
78. Emsley, P., and Cowtan, K. (2004) *Coot* : model-building tools for molecular graphics. *Acta Crystallogr. D Biol. Crystallogr.* **60**, 2126–2132
79. Pettersen, E. F., Goddard, T. D., Huang, C. C., Couch, G. S., Greenblatt, D. M., Meng, E. C., *et al.* (2004) UCSF Chimera?A visualization system for exploratory research and analysis. *J. Comput. Chem.* **25**, 1605–1612